Al-Mg-Cu based alloys and pure Al processed by high pressure torsion: the influence of alloying additions on strengthening

Jiuwen Zhang[1, 2], Nong Gao[1] and Marco J. Starink[1],

[1]Materials Research Group, School of Engineering Sciences, University of Southampton, Southampton SO17 1BJ, United Kingdom
[2]School of Materials and Engineering, Dalian University of Technology, Dalian, China, 116084

Abstract

The influence of alloying additions on strengthening of high pressure torsion (HPT) processed alloys was investigated using commercially pure Al (Al-1050 alloy) and five Al-(1-3)Mg-(0-4)Cu alloys (in wt%). Microhardness was measured on cross sections. For Al-1050 the microhardness reaches a peak at an effective strain of about 3 and subsequently decreases. The microhardness of Al-Mg-Cu alloys increases strongly and continuously with increasing equivalent strain. This workhardening rate is enhanced by increasing Mg content over the entire range of strain. Furthermore, the workhardening rates were higher in Cu-free and low Cu-containing ($\leq$ 0.4%) Al-Mg alloys as compared to high Cu-containing Al-Mg alloy at strains less than 3. The results indicate that dislocation-solute and dislocation-cluster interactions play an important role in strengthening.

Keywords: aluminium alloys; high pressure torsion; geometrically necessary dislocations; cold work; clusters

1. Introduction

Several severe plastic deformation (SPD) techniques have been applied widely to modify microstructures and produce ultra fine grained (UFG) materials with higher strength, improved formability and other favourable properties [1,2,3]. Among these techniques, considerable interest has developed in high pressure torsion (HPT) due to the advantage of refining the grain sizes of pure metals and alloys by introducing a continuous and rapid accumulation of high strain without interruption of straining. The microhardness and microstructural evolution occurring during HPT have been investigated extensively, and most attention has been paid to pure and commercially pure metals [4,5,6,7,8,9,10]. Some investigations focused on pure or high purity metals such as pure Cu [4], commercially pure Ti [5] and pure Ni [6, 7]. Pure metals are generally too weak for structural applications and therefore they are alloyed with several elements to improve its mechanical properties and inhibit grain growth. Although earlier reports, as mentioned above, described some factors influencing strengthening in pure metals and metallic alloys during SPD, there have been few systematic studies of the influence of alloying additions on strengthening in alloys during SPD.

In the present work we will investigate HPT processing of Al-Mg-Cu based alloys that have potential to be used as structural materials. The Al-Mg-Cu alloys with low Cu (<0.5wt%) content that are being studied in this work span compositions of alloys that have been widely used in beverage cans for decades [11], to compositions that are now increasingly being used as car body panels to reduce weight and thus improve fuel economy and reduce emissions [12]. In these applications they derive their

strength mostly from solution strengthening and strain hardening [13]. The Al-Mg-Cu alloys with higher Cu content (>2.5wt%) that are being studied in this work are applied predominantly in the aeronautical industry due to their in-service strength, which is due primarily to precipitation hardening [14,15,16,17], combined with good damage tolerance properties [18]. Recent development in these types of alloys has seen the introduction alloys with Li at relatively low levels (<2wt. %) [19,20,21]. These 3rd generation Al-Li alloys are now implemented on aircraft for lower wing skin, stringers, and fuselage skin as the disadvantages encountered on the first generations (reduced ductility, reduced fracture toughness and reduced thermal stability [22]) have been solved by an improvement of the chemical composition of the alloys and optimised thermo-mechanical treatments [19]. One of the alloys studied here is a low Li containing Al-Cu-Mg alloy, with composition close to those 3rd generation Al-Li alloys. In several aspects, it is the most advanced of the alloys studied, having the highest elastic modulus, the lowest density, and the highest specific fatigue resistance.

The alloys studied have a range of Mg contents. The influence of Mg content on grain refinement has been reported by Horita et al [23], who showed that the severe plastically deformed Al-3Mg had a smaller grain size about 4 times smaller than Al-1.5Mg. These effects were analysed in a model by Starink et al. [24], which indicated that the cause is the enhanced dislocation generation during SPD through addition of Mg.

The objective of the work reported here is to evaluate the influence of alloying additions on strengthening by SPD in commercially pure aluminium and five Al-(1-3)Mg-(0-4)Cu alloys (in wt %).

2. Experimental materials and procedures

Commercially pure Aluminium (Al-1050 alloy) and five Al-(1-3) Mg-(0-4) Cu alloys (in wt %) were selected for this investigation and their compositions are shown in Table 1. Prior to HPT the materials had been subjected to the following processing. The Al-1050 had been extruded into a rod with grain size of 45μm. The cast Al-1Mg, Al-1Mg-0.4Cu and Al-3Mg-0.4Cu ingots were preheated and homogenised at 540ºC, and subsequently hot rolled down to 5 mm in thickness [13]. After that, the hot rolled sheets were solution treated at 500ºC for 20 minutes, followed by cold rolling to 10% reduction, and grain size is about 30 ×100 μm. The Al-1Mg-4Cu and Al-1Mg-2.7Cu-1Li alloys (the high Cu-containing Al-Mg alloys) were cast, hot rolled to plate, solution treated and subsequently aged at room temperature to T3 condition. The specimens for HPT having a diameter of 10mm were sliced from extruded rod or rolling plate and mechanically polished to a thickness of 0.8 mm. The Al-1Mg-4Cu is within the range of the 2024 Al composition.

The HPT process was conducted on a facility with two anvils with a depression of 0.25mm in depth and 10mm in diameter, which is schematically shown in Fig. 1. The disks were held in the depression and a lubricant of MoS_2 was placed around the edges of the depression in order to reduce the friction between the upper and lower anvil. The specimens were pressed at a pressure of 3GPa and then torsion-strained at a rotation speed of 1 rpm at room temperature (RT). Samples were deformed by HPT for a total of 5 turns.

Table 1 Compositions of the alloys studied

Alloy	Composition, wt%							
	Mg	Cu	Mn	Fe	Si	Li	Zr	Al
Al-1Mg	1.02	<.01	0.25	0.22	0.16	-	-	bal.
Al-1Mg-0.4Cu	1.03	0.39	0.26	0.20	0.14	-	-	
Al-3Mg-0.4Cu	2.9	0.4	0.25	0.19	0.15	-	-	
Al-1Mg-2.7Cu-1Li	1.01	2.70	-	-	-	0.96	0.09	
Al-1Mg-4Cu	1.37	4.34	0.42	-	0.14	-	-	
Al-1050	-	0.008	0.005	0.26	0.14	-	-	

The influence of solution treatment and ageing was examined for the Al-1Mg-4Cu alloy under three types of treatments: a) 5 turns by HPT without solution and ageing treatment, b) solution heat treatment (495ºC for 30 minutes) prior to 5 turns by HPT and c) solution heat treatment (495ºC for 30 minutes) prior to 5 turns by HPT, and subsequently aged at 150ºC for 2 days.
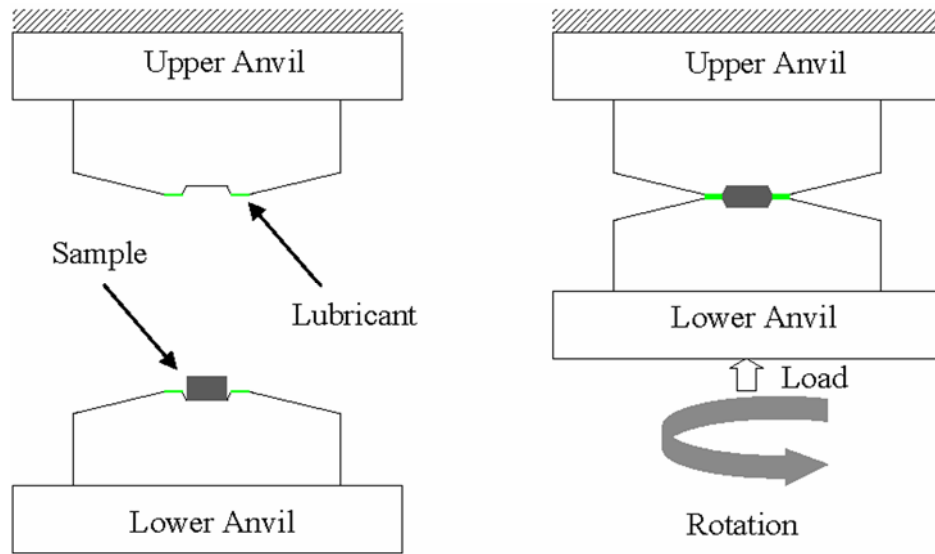

Fig. 1 Scheme of High pressure torsion tool and specimen [1]

The shear strain of disk subjected to HPT, γ, can be calculated by:

$$\gamma = 2\pi Nr / h \tag{1}$$

where N is the number of rotations, r the distance of site of microhardness measurement from the centre of the sample and h the thickness of disk. The precise true strain arising from HPT straining, and the extend to which this is homogeneous through the thickness direction, has not yet been fully understood, but we can usually use effective strain to compare the deformation in simple shear with linear strain produced by extension, drawing or rolling, because the principal shear stress acts at 45º to the plane of the principal normal stress. Thus, the true strain can be expressed as [25,26]:

$$\varepsilon = \gamma / \sqrt{3} \tag{2}$$

3

However, Eq.2 is not valid for large strain, i.e. $\gamma > 0.8$, because the directions of the maximum normal stress and strain in shear do not coincide, which can be proved by distorting a geometric square into a parallelogram and simultaneously a circle that initially inscribed in the original square into ellipse [25]. When ignoring the change in thickness of disk, the proper equation for equivalent strain at large strains is then given by [25]:

$$\varepsilon = (2/\sqrt{3})\ln[(1+\gamma^2/4)^{1/2} + \gamma/2]$$

(3)

Following HPT, disks were cut into halves in order to characterize cross sections. The sections were carefully ground up to 4000-grit SiC paper and polished to a mirror-like finish with a 0.05μm colloidal silica suspension. The Vickers microhardness, Hv, was measured at about 30 positions distributed at regular intervals across a line through the centre of cross section of the disks by imposing a load of 300g for 15s. Optical microscopy was used to observe the distribution of particles in selected Al-Mg-Cu alloys.

TEM was conducted on HPT processed Al-1050 and the Al-1Mg-4Cu alloy. The HPT processed discs were ground to a thickness of ~ 200 μm in thickness and then TEM samples of 3mm in diameter were punched out at three different regions of the disks. Subsequently, the samples were thinned to perforation using a two-jet electropolishing at -30ºC with an electrolyte solution of HNO_3: methanol =1:3 (in volume). TEM foils were examined using a JEOL 3010 microscope operating at 300 kV.

3. Results

3.1 The microhardness of HPT processed disks

Fig. 2 shows the dependence of the Vickers microhardness of the investigated specimens on distance from the centre of disks. It can be seen that the hardness of the investigated specimens depend on alloying. In general terms, the Hv values of as-received alloys increased with increasing alloying contents and the highest Hv values were recorded for the Al-1Mg-4Cu alloy. The microhardness of Al-1050 (>99.50% Al) samples after five turns by HPT initially increased from the centre to about 0.5mm from the centre and then decreased slowly (Fig. 2a). This behaviour is significantly different from that in high purity Al [27]. This could be due to the interaction of strengthening due to increasing dislocation density with increasing radii, and recovery, which becomes dominant after dislocation densities reach a particular value. The results show that very small additions of Fe and Si can lead to a significant change of shape of the Hv vs. distance curve of Al.

Fig. 2b shows that the microhardness of the three Cu-free and low Cu (0.4 wt %) Al-Mg alloys initially rapidly increases from centre to about 1mm and then slowly increases to reach a plateau near the periphery. After HPT processing, the Al-1Mg-0.4Cu alloy has a slightly higher Hv than the Al-1Mg alloy, whereas the Al-3Mg-0.4Cu has a substantially higher Hv compared with the Al-1Mg and Al-1Mg-0.4Cu alloy*s*. Fig. 2c presents the microhardness of high Cu-containing Al-Mg alloys (Al-1Mg-2.7Cu-1Li and Al-1Mg-4Cu). In the Al-1Mg-2.7Cu-1Li alloy the Hv increases approximately linearly with increasing distance from the centre, to reach a maximum of 225 Hv. In the Al-1Mg-4Cu alloy the Hv initially rapidly increases from the centre to about 2mm from the centre and then the rate slightly

decreases. No plateau can be observed near the periphery in the two high Cu-containing Al-Mg alloys and the hardness continues rising substantially up to the edge of the sample.

Fig. 2d shows the Hv increment due to HPT processing. The Hv increment for Al-1050 is larger than that for high purity Al, again highlighting the substantial influence of small additions of Fe and Si. In terms of the distribution of Hv increment, there is no clear difference between Al-1Mg and Al-1Mg-0.4Cu, whereas the higher Hv increment was observed in Al-3Mg-0.4Cu. The results show that Mg strongly increases the hardening due to HPT processing.
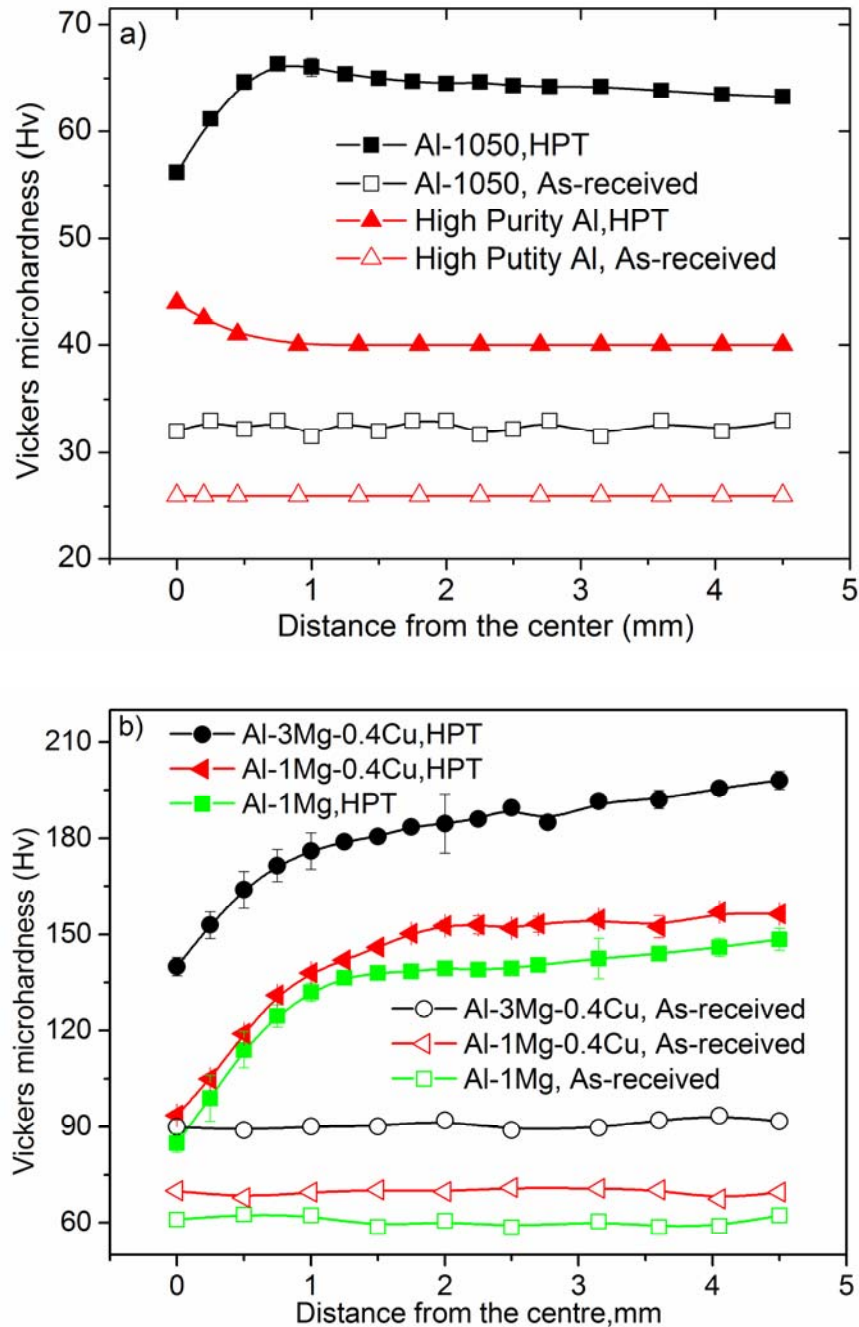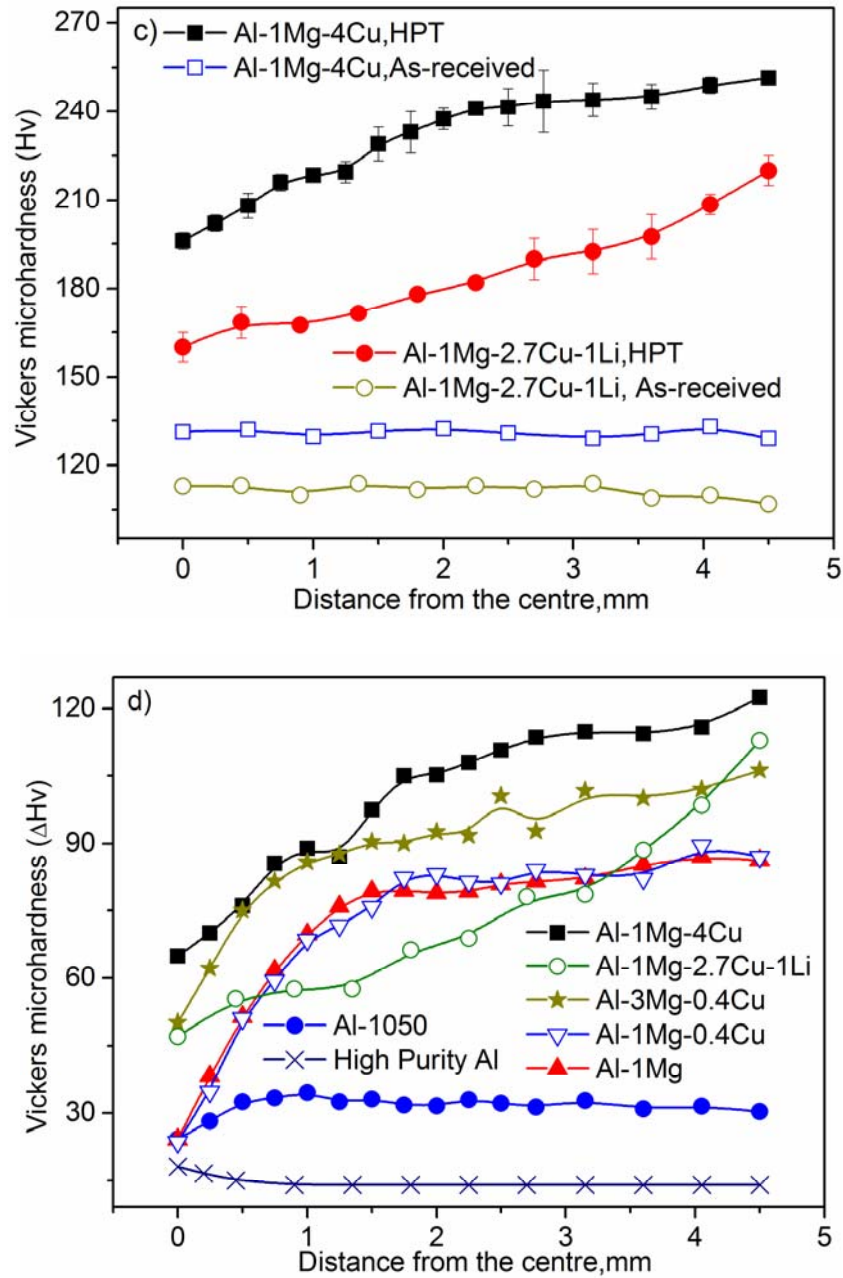
Fig. 2 Vickers microhardness vs. distance from centre of HPT disks for, a) high purity pure Al (data taken from [27]), Al-1050; b) Cu-free and low Cu-containing Al-Mg alloys; c) high Cu-containing Al-Mg alloys; d) Hv increment for all alloys studied

The influence of compression on microhardness during HPT processing was investigated for the Al-1Mg alloy. A sample was compressed at a pressure of 3GPa without torsion straining for 5 min (the duration of 5 HPT rotations) and the results show that the compression contributes to microhardness by about 3Hv.

In Cu-free and low Cu-containing alloys processed by HPT, Hv increases rapidly from centre to a radius of ~1.5mm, and hence there is substantial inhomogeneity in the mechanical properties at the central region of the disks. In the centre of the disc the strain due to rotation is zero, and only

compression contributes to deformation. However, the hardness increment in the centre (about 15-65 MPa for the alloys studied, see Fig. 2d) is much higher than that can be expected from compressive strain alone. As will be explained below, the hardening in the centre is due to the accumulation of geometrically necessary dislocations (GNDs) due to a large strain gradient. In addition, the plastic zone under the Vickers hardness tester is of finite size (indentation is a square with diagonals of about 20µm at an indentation load of 10g), and thus the hardness obtained reflects this zone. At the outer periphery, the Hv increases only slightly as a function of increasing radius.

Fig. 3 shows the dependence of the Vickers microhardness of investigated specimens on equivalent strain. In the Al-1050 alloy, the Hv vs. effective strain plot appears to become very flat across the disks. Careful observation shows that at a strain of ~ 3 a maximum in hardness occurs. The Al-Cu-Mg alloys show a slight rise of microhardness as a function of equivalent strain at relatively low equivalent strain $\varepsilon \leq 3$; however, in the strain range $\varepsilon > 3$, the HPT deformation resulted in a sharp rise of microhardness with increasing strain. A careful inspection of Fig. 3 reveals that at a relatively low equivalent strain $\varepsilon \leq 3$ the Cu-free and low Cu-containing alloys possess quicker rise of microhardness with strain than high Cu-containing alloys. Three parallel dotted lines schematically show the difference of workhardening of Al-Mg-Cu alloys in the strain range $\varepsilon < 3$. On the other hand, in the strain range $\varepsilon > 3$, the workhardening rate of Cu-free and low Cu-containing Al-Mg alloys decreased with increasing equivalent strain. By contrast, the workhardening rate of high Cu-containing alloys increased with increasing equivalent strain. These may be due to the presence of Cu-Mg co-clusters in the Al-Mg-Cu alloy [28,29] (see Discussion). Contrary to above three cases, in high purity aluminium, Hv is highest at the centre of the disc, i.e. at very small strains [27].
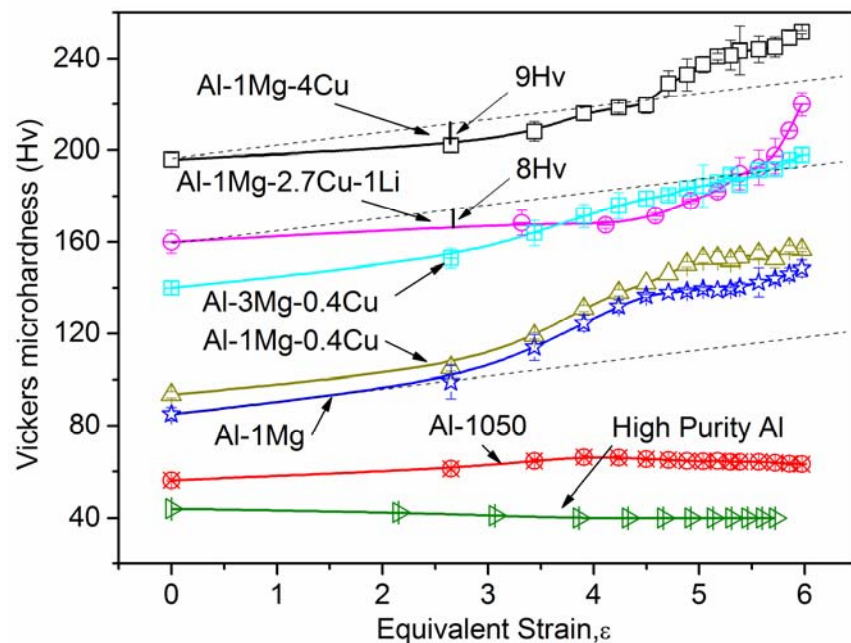

Fig. 3 Vickers microhardness vs. equivalent strain for high purity pure Al (data taken from [27]), Al-1050 and 5 Al-Mg-Cu based alloys processed by HPT. The dotted parallel lines are guides to show averaged trends.

3.2 Microstructural observations of disks subjected to HPT

Fig. 4 shows an optical micrograph of the Al-1Mg-4Cu alloy deformed by HPT to 5 turns. The lower surface and upper surface of disk are designated on the graph by mark L and U. They are contacted with the lower anvil (rotating) and upper anvil (stable) of the HPT machine when the disk is deformed. The grain boundaries are not visible in this optical micrograph of a lightly etched specimen. Instead, the observed contrast is mainly due to intermetallic particles in the alloy. Earlier work has identified these particles as Al_7Cu_2Fe and Al_2CuMg [30,31,32]. Fig. 4 shows that the HPT produced a redistribution of intermetallic particles which were initially in straight bands parallel to the rolling direction, which is in the plane of the HPT disc. The microstructure can broadly be classified into 3 different deformation zones according the particle size and the direction of banded distribution of particle: a zone with coarser nonuniform particles (marked by A), a zone with finer uniform particles (marked by C) and a transition zone (marked by B). Moreover, there are slightly different contrast between optical microstructures of two half cross sections.

It is very interesting to note that the patterns of bands of intermetallic particles are always at an angle to what are often implicitly assumed to be the symmetry axes of torsional rotation. The present results show that in contrast to these assumptions in earlier works on HPT, deformation depends not just on distance from the axis of rotation but also on distance from the lower platen.

Fig. 4 Optical microstructure of a cross section of the Al-1Mg-4Cu disk subjected to HPT. L denotes lower surface and U denotes upper surface.

The TEM micrographs of Al-1050 alloy at about 1 mm (ε_{eq} = 4.2), 2.5 mm (ε_{eq} = 5.3) and 4 mm (ε_{eq} = 5.8) from the centre of disk are shown in Fig. 5a-c, respectively. The HPT processed samples show slightly different structure from centre to outer region of disk. From Fig. 5a it can be observed that there are some very fine grains with a size of about 100-200nm, and the grain boundaries are curved and wavy. A high dislocation density was observed at grain boundaries and inside some grains (Fig. 5a). Averaging over several TEM micrographs provided a grain size of 0.6μm in the centre. At effective strain 5.3 (Fig. 5b), somewhat larger grains and lower density of dislocations was observed. Free dislocation density at grain boundaries and distortions and bending of the lattice fringes were observed at the 4mm position (Fig. 5c).
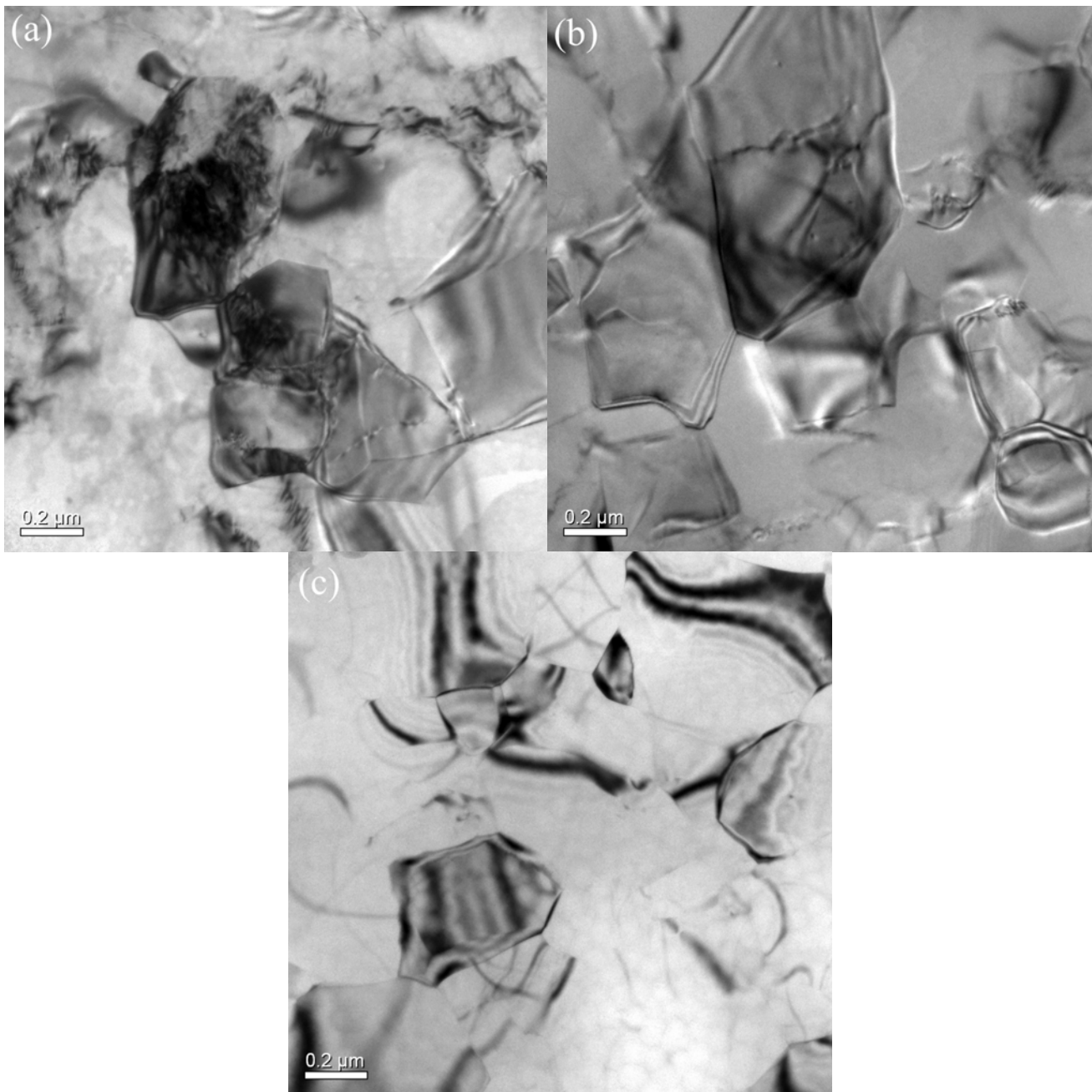
Fig. 5 TEM of Al-1050 by m-HPT for 5 turns: a) at 1mm from the centre of the disk ($\varepsilon_{eq} \approx 4.2$); b) at 2.5mm from the centre of the disk ($\varepsilon_{eq} \approx 5.3$); c) at 4mm from the centre of the disk ($\varepsilon_{eq} \approx 5.8$)

Fig. 6 shows the typical TEM microstructure observations of Al-1Mg-4Cu samples after HPT straining under different heat treatment conditions. The TEM graphs were taken at the region about 4 mm away from the disk centre ($\varepsilon_{eq} = 5.8$). HPT introduced a high density of dislocations in the Al-1Mg-4Cu alloy (Fig. 6a) and the grain boundaries were often ill-defined. Fig. 6b shows the TEM microstructure adjacent to the centre of disk at about 1mm ($\varepsilon_{eq} = 4.2$). At this location a large grain consisting of several subgrains with near parallel subgrain boundaries were observed. In order to investigate the thermal stability and the influence of HPT straining on precipitates, additional experiments were conducted. It can be seen that the microstructure subjected to solution treatment at 495ºC for 30

9

minutes prior to HPT is similar to the results without solution treatment. It is difficult to define grain size from TEM graphs (Fig. 6a and c). Another disk was subjected to solution heat treatment (495ºC for 30 minutes) and subsequently processed to 5 turns by HPT and then aged at 150 ºC for 2 days. The TEM microstructure shown in Fig. 6d reveals dislocation cells and dislocation-tangles in the heavily deformed grains of the alloy. The ageing at 150ºC appeared to have caused a decrease in the dislocation density. In this image, the grain size was estimated to be about 300 nm. Grain boundaries are mostly poorly defined, but some grain boundaries are identifiable and a portion of these are still curved or wavy, which indicate a non-equilibrium state [23].

4. Discussion

The results show that whilst HPT processing increased hardness in all alloys, the magnitude and rate of this increase is strongly influenced by alloying additions over a wide range of strain.

4.1 The evolution of microstructure in pure Al during HPT

Prior to HPT, Al-1050 has low hardness (~30 Hv), and the limited strengthening compared to high purity Al is predominantly due to solid solution strengthening. After HPT, the grain was dramatically refined and the hardness was increased. The central and outer regions of the HPT disk (Fig. 5) show markedly different microstructures. Elongated grains are typical results of monotonic HPT straining [33] and ECAP [34] especially with deformation route C. It is well known that both the applied pressure (P) and the number of revolutions (N) influence the development of microhardness in HPT [5, 7] and larger numbers of turns and/or higher pressure applied to disks can produce a more homogeneous microstructure.

It is instructive to compare the results obtained on Al-1050 in this investigation after rotation by HPT for 5 turns with data reported earlier for other pure metals. In the literature, the grain size measured for pure (99.96%) Cu deformed by HPT (*P*=6GPa, *N*=5) is 440nm in the centre region and 200nm in the outer region [35], and few coarse grains were also observed in higher purity Cu (99.98%) [4]. The grain size of pure (≥99.98%) Ni deformed by HPT (*P*=9GPa, *N*=5) increased from 200nm in the centre (ε_{eq} ≅ 4.2) to 400nm at the edges (ε_{eq} ≅ 5.8) [7], and other studies using 0.3mm thick disks showed finer grain sizes of 200nm (*P*=7GPa, *N*=5) [36] and 260nm (*P*=6GPa, *N*=5) [6] at the periphery (equivalent strain of about 7); and for CP Ti Grade 4 subjected to HPT (*P*=6, *N*=10), the grain size is about 160nm [37]. All of the above mentioned grain sizes were recalculated by the method described in [38] and these pure metals attained a much finer grain size than high purity Al or our HPT processed Al-1050 alloy.

From the analysis of the TEM micrograph of Al-1050 alloy (Fig. 5), it is important to note that the density of dislocations at grain boundaries decreased with an increasing strain along the radius of disks, which suggest that the annihilation of dislocations in the periphery of disk is faster than in the centre area during HPT processing. This could be related to the presence of geometrically necessary dislocations which are generated to accommodate the strain gradient (implying lattice curvature)

resulting from strain gradient during HPT processing. GNDs carry the same sign, which can not be mutually annihilated. At the centre region, the GNDs govern the hardening. At the outer region, the saturation of hardness was related to a saturation of total density of dislocation, in which the large sum of statistical stored dislocation (SSDs) with opposite signs can easily annihilate due to high stacking fault energy. Thus, these are believed to be responsible for the corresponding increase in grain sizes with increasing strain along the radius of disks subjected to HPT.
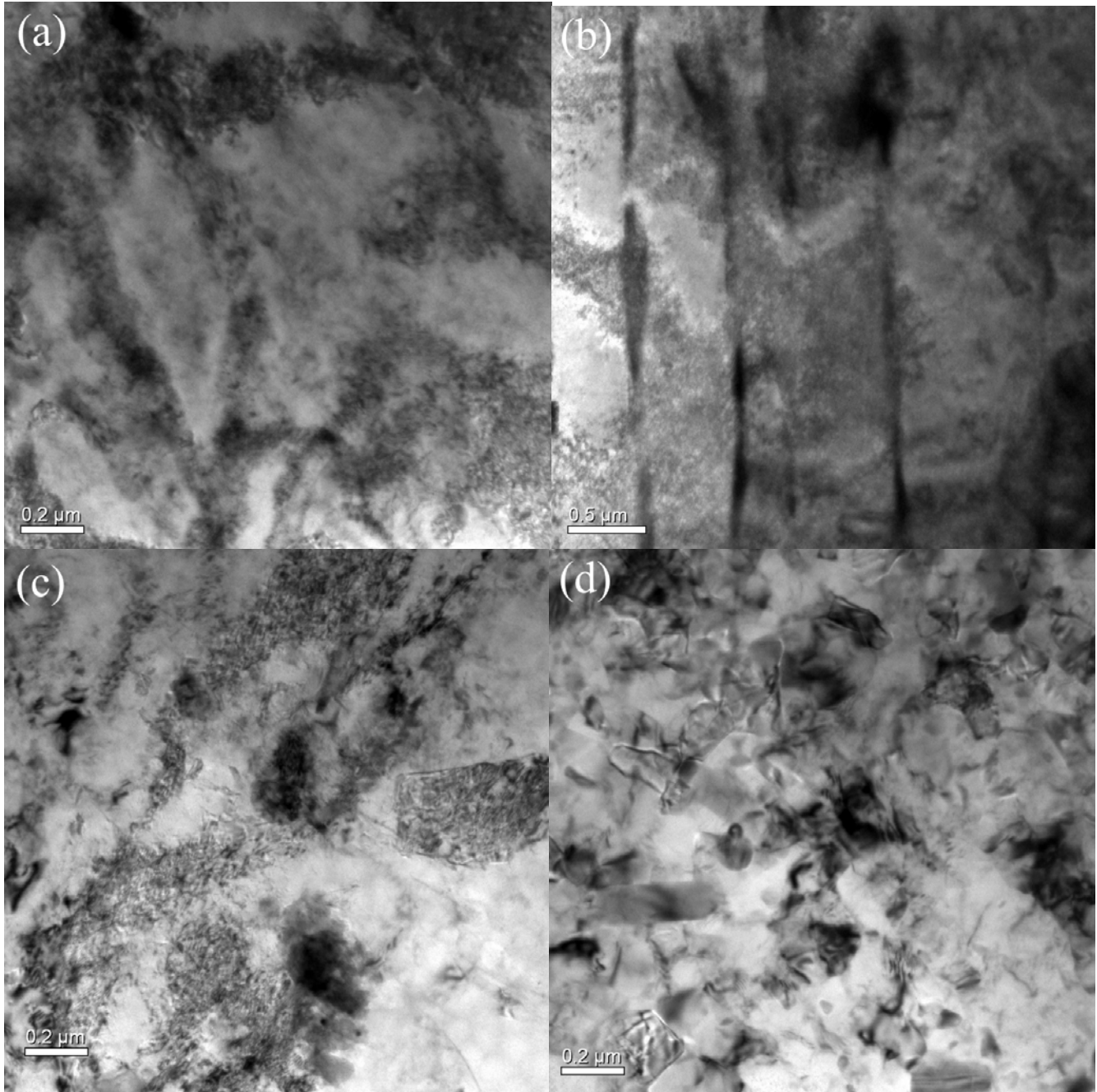

Fig. 6 Dislocation structures of the Al-1Mg-4Cu alloy at 4 mm from the centre of the disk: a) after 5 turns HPT ($\varepsilon_{eq} \approx 5.8$); b) large grain with subgrains after 5 turns HPT ($\varepsilon_{eq} \approx 4.2$); c) after 495ºC solution treatment for 30 minutes+ 5 turns HPT ($\varepsilon_{eq} \approx 4.2$); d) after 495ºC solution treatment for 30 minutes + 5 turns HPT + 150 ºC ageing for 2 days ($\varepsilon_{eq} \approx 5.8$)

In this work, higher dislocation density was observed in the centre of Al-1050 alloy compared with high purity aluminium [27]. This could be due to a low volume of intermetallic phases at grain boundaries in the 1XXX series Al alloy, which are binary Al_xFe and ternary Al-Fe-Si [39,40]. These particles can be broken up and a low volume fraction of Al-Fe-Si precipitates were also observed after ECAP [41], which may inhibit the movement of dislocation during severe plastic deformation. In addition, they may be partially dissolved during SPD. Supporting the latter is the observation by Korchef et al. [42] that the lattice parameter of the Al-rich phase in Al 1100 alloy decreased during ECAP processing, which may be due to the dissolution of elements such as Si and Fe.

4.2 The evolution of microstructure in Al-Mg-Cu alloys during HPT

Addition of 0.4wt% Cu to Al-1Mg causes a small improvement in strength and hardness both in solution treated and subsequently rolled condition (see [13]). The present results also show that after severe plastic deformation using HPT, the Cu addition increases hardness slightly (Fig. 2b). The magnitude of this difference seems to be independent of strain. However, increasing the Mg content from 1 to 3 wt% causes a much stronger rise of microhardness, which indicates Mg addition can effectively improve strengthening during HPT processing. Previous studies reported that the strength of Al-Mg-Cu alloys increases approximation linearly with Mg content [13, 24]. In the present SPD alloys also the interaction between Mg content and dislocations is important. High density of dislocations have been widely observed in Al-Mg alloys subjected to ECAP and the density increased with increasing Mg content [43]. A previous study [44], showed that an Al-Mg-Sc-Zr alloy processed by HPT up to half turn contains a high density of dislocations ($16 \cdot 10^{14} m^{-2}$) in the periphery of disk (having a radius of 15mm and a thickness of 0.5mm), which did not significantly change on increasing straining beyond five turns. In fact, Horita et al. [23] also reported the grain boundaries in Al-Mg alloys produced by severe plastic deformation are in high-energy nonequilibrium configuration.

In the present investigations, the major difference observed between the low Cu-containing Al-Mg alloys and high Cu-containing Al-Mg alloys was the rate of workhardening, which was faster in the lower Cu-containing Al-Mg alloys during initial stages of strain (less than 3) and slower at higher strain levels (strains in excess of 3). Our high Cu-containing Al-Mg alloys processed to 5 turns show a consistently fast increase over a wide range from the centre to edge of HPT processed disk and no saturation of hardness was observed under the present conditions. This is different from many other alloys (e.g. austenitic steel and a titanium [9,45]), where saturation occurred near the periphery of disks processed for at least 2 turns. The optical microscopy of Al-1Mg-4Cu (Fig. 4) combined with Hv distribution along the diameter (Fig. 2), suggests that the alloy exhibits significant inhomogeneity after HPT for 5 turns, where the sizes of intermetallics decreased gradually with increasing distance from the centre. TEM results (Fig. 6a and d) also demonstrated that there exists significant difference in microstructure between different areas.

Some of the strengthening effects, especially in the alloys with significant Cu, will be due to nanoscale precipitates. There have been some controversies over the precipitates in these Al-Cu-Mg alloys regarding to the ageing sequence and crystal structure, but recent work has demonstrated that Cu-Mg clusters dominate the strengthening during the initial ageing including room temperature aged alloys [29]. (Mg-Cu co-clusters can not be resolved in TEM, but can be resolved by 3 dimensional atom probe [29,46,47].) Although the HPT processed Al-1Mg-4Cu alloy has a high dislocation density which might stimulate nucleation of semicoherent precipitates (S or S' phase [14,48]), no such precipitates were observed in the aged Al-1Mg-4Cu sample. Hence the Cu-Mg clusters played an important role in strengthening of Al-1Mg-4Cu subjected to HPT.

Compared with low Cu-containing Al-Mg alloys, there seems to be only a limited strengthening effect in Al-1Mg-2.7Cu by HPT over intermediate strain range. This may be explained by the interaction of co-clusters and dislocation during deformation, as follows. The order strengthening effect from co-cluster can be approximated as [29]:

$$\Delta\tau_{SRO} = \frac{\gamma_{SRO}}{b} = \frac{\Delta H_{A-B}}{b^3} \times \frac{4}{\sqrt{3}}\left[\frac{2}{3}(y_A + y_B) - (\frac{2}{3}x_B y_A + \frac{2}{3}x_A y_B + 2x_A x_B)\right] \qquad (4)$$

where γ_{SRO} is the change in energy per unit area on slip planes, ΔH_{A-B}, the enthalpy of the nearest neighbour bond, y_A, the amount of A atoms in the co-clusters, y_B, the amount of B atoms in the co-clusters, x_A, the amount of A atoms in the Al-rich phase, x_B, the amount of B atoms in the Al-rich phase. It was demonstrated [29] that in Al-Mg-Cu alloys the Cu-Mg co-clusters can form very quickly and harden the alloy. The strengthening for the present Al-1M-Cu alloy is about 300MPa. At the onset of straining, the Cu-Mg co-clusters, inhibit the movement of dislocations, increasing the strength. However, co-clusters are shearable, and as straining proceeds, the moving dislocations will destroy Cu-Mg co-clusters (and to a lesser extend may generate some new ones). The net effect is a decrease in the strengthening contribution due to co-clusters. This effect is thought to be the main cause for the limited work hardening in the strain range up to about 4 in the alloys containing substantial Cu (see Fig. 3). In this view the continuous destruction of co-clusters is completed at strain of about 4, and hence on further increase of strain an increased work hardening will occur. The latter is evident in Fig. 3.

Conclusions

In the present study, the influence of alloying additions on strengthening in high pressure torsion (HPT) process was investigated using pure Al (Al-1050 alloy) and five Al-(1-3)Mg-(0-4)Cu alloys (in wt%). The Vickers microhardness was measured along diameters in each disk and the microstructural changes were studied in the Al-1050 and Al-1Mg-4Cu alloys. The following main conclusions can be drawn:

The microhardness of the Al-1050 aluminium alloy subjected to HPT reaches a peak at a strain of about 3 and subsequently decreases. The smaller grain size was observed in centre region of disk.

The microhardness of Al-Mg-Cu alloys increases drastically and continuously with increasing equivalent strain and Mg increases the workhardening rate of the Al-Mg-Cu alloys over the entire range of strain.

The hardness of two high Cu-containing Al-Mg alloys increases approximately linearly with the distance from centre of disk. At stains less than 3, the workhardening rates were higher in Cu-free and low Cu-containing Al-Mg alloy than in high Cu-containing Al-Mg alloy. By contrast, as straining proceeds, higher workhardening rates were observed in high Cu-containing Al-Mg-Cu alloys. The differences indicate the existence of Cu-Mg co-clusters influence the strengthening effect of Al-Mg-Cu alloy during HPT processing.

References

[1]   A.P. Zhilyaev, T.G. Langdon, Prog. Mater. Sci. 53 (2008) 893-979.
[2]   R.Z. Valiev, T.G. Langdon, Prog. Mater. Sci. 51 (2006) 881-981.
[3]   N. Tsuji, Y. Saito, H. Utsunomiya, S. Tanigawa, Scripta Mater. 40 (1999) 795-800.
[4]   N. Lugo, N. Llorca, J.M, Cabrera, Z. Horita, Mater. Sci. Eng. A 477 (2008) 366-371.
[5]   Y. Todaka, M. Umemoto, A. Yamazaki, J. Sasaki, K.Tsuchiya, Mater. Trans. 49 (2008) 7-14.
[6]   Z.Q. Yang, U. Welzel, Mater. Letter 59 (2005) 3406-3409.
[7]   A.P. Zhilyaev, G.V. Nurislamova, B.K. Kim, M.D. Baro, J.A. Szpunar, T.G. Langdon, Acta Mater. 51 (2003) 753-765.
[8]   F. Wetscher, A. Vorhauer, R. Pippan, Mater. Sci. Eng. A 410 (2005) 213-216.
[9]   A. Vorhauer, R. Pippan, Scr. Mater. 51 (2004) 921-925.
[10]   J.M. Garcia-Infanta, A.P. Zhilyaev, A. Sharafutdinov, O.A. Ruano, F. Carreno, J. Alloys Compounds 473 (2009) 163-166.
[11]   J. Courbon, Scripta Mater. 48 (2003) 1519 -1524.
[12]   G.B.Burger, A.K. Gupta, P.W. Jeffrey, D.J. Lloyd, Mater. Charact. 35 (1995) 23.
[13]   Z. Zhu, M.J. Starink, Mater. Sci. Eng. A 488 (2008) 125-133.
[14]   S.C. Wang, M.J. Starink, N. Gao, Scripta Mater. 54 (2006) 287-291.
[15]   M.J. Starink, P. Wang, I. Sinclair, P.J. Gregson, Acta Mater. 47 (1999) 3841-3853.
[16]   I.N. Khan, M.J. Starink, J.L. Yan, Mater. Sci. Eng. A 472 (2008) 66-74.
[17]   N. Gao, M.J. Starink, L. Davin, A. Cerezo, S.C. Wang,P.J., Mater. Sci. Tech. 21 (2005) 1010-1018.
[18]   N. Kamp, N. Gao, M.J. Starink, I. Sinclair, Int. J. Fatigue 29 (2007) 869-878.
[19]   C. Giummarra, B. Thomas, R.J. Rioja. Proceedings of the Light Metals Technology Conference 2007, Canada.
[20]   M.A. Munoz-Morris, I. Gutierrez-Urrutia, N. Calderon, D.G. Morris, Mater. Sci. Eng. A 492 (2008) 268-275.
[21]   M.J. Starink, N. Gao, N. Kamp, S.C. Wang, P.D. Pitcher, I. Sinclair, Mater. Sci. Eng. A 418 (2006) 241-249.
[22]   M.J. Starink, A.J. Hobson, I. Sinclair, P.J. Gregson, Mater. Sci. Eng. A 289 (2000) 130-142.
[23]   Z. Horita, S.J. David, F. Minoru, N. Minoru, R.Z. Valiev, T.G. Langdon, J. Mater. Res. 11(1996) 1880-1890.
[24]   Z. Zhu, M.J. Starink, Mater. Sci. Eng. A 489 (2008) 138-149.
[25]   N.H. Polakowski, E.J. Ripling, Strength and structure of engineering materials, Englewood Cliffs, NJ: Prentice-Hall, 1966.
[26]   R.Z. Valiev, Y.V. Ivanisenko, E.F. Rauch, B. Baudelet, Acta Mater. 44 (1996) 4705-4712.
[27]   X. Cheng, Z. Horita, T.G. Langdon, Acta Mater. 56 (2008) 5168-5176.
[28]   S.P Ringer, K. Hono, T. Sakurai, I.J. Polmear, Scripta Mater. 36 (1997) 517-521.
[29]   M.J. Starink, S.C. Wang, Acta Mater. 57 (2009) 2376-2389.
[30]   S.C. Wang, F. Lefebvre, J.L. Yan, I. Sinclair, M.J. Starink, Mater. Sci. Eng. A 431 (2006) 123-136.
[31]   S.C. Wang, M.J. Starink, Int. Mater. Rev. 50 (2005) 193-215.
[32]   M.J. Starink, S.C. Wang, Scripta Mater., in press (2010).
[33]   A.M. Andrei, B.S. Boris, G.P. Svetlana, V.D. Sergei, B. Brigitte, J. Mater. Sci. 43 (2008) 3800-3805.
[34]   A. Mishra, B.K. Kad, F. Gregori, M.A. Meyers, Acta Mater. 55 (2007) 13-28.
[35]   Z. Horita, T.G. Langdon, Mater. Sci. Eng. A 410 (2005) 422-425.
[36]   B. Baretzky, M. D. Baró, G. P. Grabovetskaya, J. Gubicza, M. B. Ivanov, Yu.R. Kolobov, T.G. Langdon, J. Lendvai, A. G. Lipnitskii, A.A. Mazilkin, A.A. Nazarov, J. Nogués, I.A. Ovidko, S.

G. Protasova, G.I. Raab, Á. Révész, N.V. Skiba, J. Sort, M.J. Starink, B.B. Straumal, S. Suriñach, T. Ungár and A.P. Zhilyaev, Rev. Adv. Mater. Sci. 9 (2005) 45-108.

[37]   R.K. Islamgaliev, V.U. Kazyhanov, L.O. Shestakova, A.V. Sharafutdinov, R.Z. Valiev, Mater. Sci. Eng. A 493(2008) 190-194.

[38]   M.J. Starink, X.G. Qiao, J.W. Zhang, N. Gao. Acta Mater. 57(2009), 5796-5811.

[39]   P. Skjerpe, J. Gjonnes, Y. Langsrud, Ultramicroscopy, 22 (1986) 239-249.

[40]   M.W. Meredith, J. Worth, R.G. Hamerton, Mater. Sci. Forum 396-402 (2000) 107-112,

[41]   A. Korchef, N. Nabil, C. Yannick, G. Sandrine, L. Cédric, M. Jalel, K. Abdelwaheb, Adv. Eng. Mater. 6 (2004) 222-228.

[42]   A. Korchef, N. Nabil, A.W. Kolsi, Cryst. Res. Tech. 44 (2009) 106-110.

[43]   D. Markus, P. Florian, M. Johannes, H.H. Werner, J. Mater. Sci. 43 (2008) 7481-7487.

[44]   D. Fatay, E. Bastarash, K. Nyilas, S. Dobatkin, J. Gubicza, T. Ungar, Mater. Res. Adv. Tech. 94 (2003) 842-847.

[45]   Y. Todaka, M. Umemoto, A. Yamazaki, J. Sasaki, K. Tsuchiya, Mater. Trans. 49 (2008) 47-53.

[46]   M.J. Starink, N. Gao, L. Davin, J. Yan, A. Cerezo, Philosoph. Mag. 85 (2005) 1395.

[47]   R.K.W. Marceau, G. Sha, S.P. Ringer, in Aluminium Alloys - Their Physical and Mechanical Properties, Volume 1. J. Hirsch, B. Strotzki, G. Gottstein (Eds.), Wiley-VCH Verlag GmbH & Co. KGaA, Weinheim, 2008, pp. 83-90

[48]   S.C. Wang, M.J. Starink, Acta Mater. 55 (2007) 933-941.